Sparsity-Enforced Microwave Inverse Scattering using Soft Shrinkage Thresholding

Hidayet Zaimaga
Laboratoire des signaux et systèmes-UMR8506
(CNRS-CentraleSupélec-Univ.Paris-Sud)
Email:hidayet.zaimaga@l2s.centralesupelec.fr

Marc Lambert
GeePs | Group of electrical engineering - Paris, UMR CNRS 8507,
CentraleSupélec, Univ. Paris-Sud, Université Paris-Saclay,
Sorbonne Universités, UPMC Univ Paris 06
Email:Marc.Lambert@geeps.centralesupelec.fr

***Abstract*—A sparse nonlinear inverse scattering problem arising in microwave imaging is analyzed and numerically solved for retrieving dielectric contrast of region of interest from measured fields. The proposed approach is motivated by a Tikhonov functional incorporating a sparsity promoting l_1-penalty term. The proposed iterative algorithm of soft shrinkage type enforces the sparsity constraint at each nonlinear iteration and provides an effective reconstructions of unknown (complex) dielectric profiles. The scheme produces sharp and good reconstruction of dielectric profiles in sparse domains and keeps its convergence during the reconstruction. Numerical results present the effectiveness and accuracy of the proposed method.**

I. Introduction

Development of efficient methods and techniques for solving inverse electromagnetic scattering problems has been widely emerged in recent years. High demand of such methods in various applications such as material characterization, subsurface prospecting, remote sensing, and non-destructive testing and evaluation [1], [2] enforces the importance and the need of effective and accurate methods. Inverse electromagnetic scattering problems reconstruct material properties such as permittivity and conductivity in an unknown region from measured electromagnetic fields. However, implementation of such stable, reliable, and efficient reconstruction algorithms is challenging because of the nonlinearity of the scattering equations and ill-posedness of the problem [1], [3], [4].

Several approaches have been proposed in order to overcome these issues. Global optimization tools, multi-step information retrieval techniques, and qualitative methods have been introduced to alleviate the non-linearity or its effects. Moreover, first order approximations such as diffraction tomography, Born and Rytov approximations have been proven in order to linearize the problem [1], [3], [5]. On the other hand, innovative sparseness-regularized formulations have recently emerged as an effective recipe to overcome the non-uniqueness and/or numerical instability of the inversion process [6], [7]. The reason behind this is that many images have sparse representations with respect to their expansion basis in the wavelet domain and this yields new developing approaches that minimize the cost functions with zeroth/first norm penalty terms using highly effective iterative shrinkage thresholding algorithms. Such an increased interest is proven by number of publications in wide domains [4], [6], [7], [8], [9], [10].

In this work, sparsity constraint is directly applied to the problem of reconstructing the complex internal dielectric properties of an object based on knowledge of the external scattered field which is generated by the interaction between the object and a known incident field. The nonlinear optimization problem is solved by iterative algorithm of soft shrinkage in order to enforce the sparsity constraint. Sparsity is applied in each iteration by a soft thresholding function. The proposed method provides necessary and sufficient conditions to yield well-posedness and convergence by adding smoothness as well [11], [12], [13].

II. Problem Statement and Discretization

We consider a 2D configuration with transverse magnetic polarization (TM) case where the object under investigation illuminated by a given source numbered as $i, i = 1, ..., Ns$ as in Fig.1. A source generates an incident electric field E^{inc} which is polarized along the z-axis with an implicit time factor $\exp(-\mathrm{i}\omega t)$. The object is considered in an investigation domain D and the different media are characterized by their propagation constant $k(\mathbf{r})$ such that $k(\mathbf{r})^2 = \omega^2\varepsilon_0\varepsilon_r(\mathbf{r})\mu_0 + \mathrm{i}\omega\mu_0\sigma(\mathbf{r})$, where ω is the angular frequency, ε_0 and μ_0 are the permittivity and the permeability of the air respectively, $\varepsilon_r(\mathbf{r})$ and $\sigma(\mathbf{r})$ are the relative permittivity and conductivity of the medium as $\mathbf{r} \in D$ is an observation point. The dielectric properties of D are described by the inhomogeneous contrast function, $\chi(\mathbf{r})$, which is defined for non-magnetic area such as $\chi(\mathbf{r}) = \left(k(\mathbf{r})^2 - k_B^2\right)$ where k_B is the propagation constant of the embedding medium.

A known incident field E^{inc} interacts with the scatterer yielding to a total field which is the sum of the incident and scattered fields. The direct scattering problem is to obtain the total field from the dielectric properties of the investigation domain, and then the scattered field at the detectors. The inverse scattering problem is to retrieve the contrast function of the region D from the measurements of the scattered fields at the detectors. We also define the contrast source induced within the object by the incident wave such as $J(\mathbf{r}) = \chi(\mathbf{r})E^{\text{tot}}(\mathbf{r})$, E^{tot} being the total field in the object. Assuming no magnetic media and considering the boundary and radiation conditions we can obtain two coupled contrast source integral equations

978-0-9928-6265-7/16/$31.00 ©2016 IEEE

by applying Green's theorem to Helmholtz wave equations [2], [5] as following

$$E^{\text{tot}}(\mathbf{r}) = E^{\text{inc}}(\mathbf{r}) + \int_D G(\mathbf{r},\mathbf{r}\,')\chi(\mathbf{r}\,')E^{\text{tot}}(\mathbf{r}\,')d\mathbf{r}\,' \quad \forall \mathbf{r} \in D \tag{1}$$

$$E^{\text{diff}}(\mathbf{r}) = \int_D G(\mathbf{r},\mathbf{r}\,')\chi(\mathbf{r}\,')E^{\text{tot}}(\mathbf{r}\,')d\mathbf{r}\,' \quad \forall \mathbf{r} \in L \tag{2}$$

where $G(\mathbf{r},\mathbf{r}\,') = \frac{\mathrm{i}}{4}\mathrm{H}_0^{(1)}\left(k_B\|\mathbf{r}-\mathbf{r}\,'\|\right)$ and $\mathrm{H}_0^{(1)}$ is the 0-th order Hankel function of the first kind and E^{diff} is the scattered field. Solving the equations (1) and (2) the unknown contrast function can be determined. Following this, the scattering equations are discretized with the point-matching Method of Moments as in [5] by considering pixel basis functions

$$\psi_k(\mathbf{r}) = \begin{cases} 1 & \mathbf{r} \in D_k, \\ 0 & \text{otherwise}, \end{cases} \tag{3}$$

D_k being the $k-$th pixel and the unknown contrast, $\chi(\mathbf{r}) = \sum_{k=1}^{N}\chi_k\psi_k(\mathbf{r})$ becomes sparse.

III. Nonlinear Optimization

Soft shrinkage is an approach which minimizes a nonlinear Tikhonov functional with sparsity promoting penalty term. The algorithm is based on the iterated soft shrinkage approach originated for linear operators in the work [6]. A generalization to nonlinear inverse problems has been studied in [4], [14].

The algorithm performs a gradient descent step which involves the adjoint gradient of the cost function with a step size τ, like Landweber method, and then a shrinkage step. The latter enforces the sparsity of the reconstruction by setting the small coefficients to zero. Following this, BB method is suggested to choose the step size in order to overcome the slow convergence of the iterative soft shrinkage algorithm. The solution of the inverse problem can be obtained by minimizing the cost function which is an error between the measured quantity and the solution obtained by a forward problem. Cost function to be minimized is of the form

$$F(\chi) = \frac{1}{2}\left\|\zeta(\chi) - E^{\text{diff}}\right\|^2 + \alpha\|\chi\|_{l_1} \tag{4}$$

whereas $\zeta(\chi) = G(\mathbf{r},\mathbf{r}\,')\chi(\mathbf{r}\,')[I - G(\mathbf{r},\mathbf{r}\,')\chi(\mathbf{r})]^{-1}E^{\text{inc}}$. The l_1 penalty can promote a-priori knowledge of the sparse representation.

Iterative soft shrinkage has the form as

$$F(\chi) = \underbrace{\frac{1}{2}\left\|\zeta(\chi) - E^{\text{diff}}\right\|^2}_{K(\chi)} + \alpha\|\chi\|_{l_1} \tag{5}$$

where $\zeta : X \mapsto Y$ is a bounded and nonlinear operator with respect to unknown contrast χ. At first, the algorithm has started by choosing an initial guess χ^1, and the iteration continues as

$$\chi^{k+1} = S_\alpha\Big(\chi^k - \tau\zeta^{'*}(\chi^k)\Big[\zeta(\chi^k) - E^{\text{diff}}\Big]\Big) \tag{6}$$

where τ is the step size, $\zeta'(\chi)$ is the gradient of nonlinear function $\zeta(\chi)$, and $\zeta^{'*}(\chi)$ is the adjoint operator. S_α is the soft shrinkage operator defined componentwise by [6]

$$(S_\alpha(\chi))_i = \begin{cases} (|\chi_i| - \alpha)\text{sign}(\chi_i), & \text{if} \quad |\chi_i| > \alpha \\ 0, & \text{otherwise.} \end{cases} \tag{7}$$

The term $\zeta^{'*}(\chi^k)\Big[\zeta(\chi^k) - E^{\text{diff}}\Big]$ is the gradient of the discrepancy $\frac{1}{2}\left\|\zeta(\chi) - E^{\text{diff}}\right\|^2$. The algorithm which has been computed is shown in Algorithm.1.

Algorithm 1 Steepest descent reconstruction algorithm with sparsity constraint

1: Initialize χ^1 and α
2: **for** $k = 1, \cdots, K$ **do**
3: Solve the direct problem $E^{\text{diff}}\left(\chi^k\right)$
4: Compute the gradient $K'\left(\chi^k\right) = \nabla_\chi K\left(\chi\right)|_{\chi^k}$
5: Smooth the gradient $K_s'\left(\chi^k\right)$
6: Determine the step size τ_k
7: Update inhomogeneity by $\chi^{k+1} = \chi^k - \tau_k K_s'\left(\chi^k\right)$
8: Threshold χ^{k+1} by $S_\alpha\left(\chi^{k+1}\right)$
9: check stopping criterion
10: **end for**
11: **output** approximate the minimizer of (5).

1) Gradient K_s': The main idea is to obtain the gradient (Frechet derivative) of the whole discrepancy term by adjoint method and avoid calculating $\zeta'^*(\chi)$. It is emerged in practice that the gradient $K'(\chi)$ has unnatural oscillating properties and using smoother gradient can prevent these oscillations. This process is also called denoising [7], [12], [13]. Therefore, we look for a Sobolev smoothed gradient $K_s'(\chi)$ by solving

$$K_s'(\chi)\zeta = (\delta I - \beta\Delta)^{-1}K'(\chi)\zeta, \tag{8}$$

where I refers to the identity, Δ refers to the Laplacian operator [15]. A proper choice of the weighting parameters δ and β will allow us to drive the regularization properties of our algorithm in an efficient and predictable way. For theoretical justification we refer to [13].

2) Step Size Selection: Selecting the step size adaptively can increase the convergence speed. Therefore, the step size τ can be determined in order to fasten the algorithm. The iterative soft shrinkage algorithm with a fixed step size favors the classical Landweber method. Thus, the motivation for increasing the rate of convergence is the comparison with the classical Landweber iteration whose slow convergence results from using a constant step size which is very small [4], [9]. Hence, we select the step size in a way to increase the convergence speed where we consider only the steepest descent operation $\chi^k - \tau K_s'(\chi^k)$ of the algorithm. The selection is

done by the two-point rule of Barzilai and Borwein which calculates the step size as [16]

$$\tau_k = \frac{\left\langle \chi^k - \chi^{k-1}, K_s'\left(\chi^k\right) - K_s'\left(\chi^{k-1}\right)\right\rangle}{\left\langle K_s'\left(\chi^k\right) - K_s'\left(\chi^{k-1}\right), K_s'\left(\chi^k\right) - K_s'\left(\chi^{k-1}\right)\right\rangle}. \quad (9)$$

In the implementation we use this step size as an initial guess and it is decreased geometrically until the Armijo condition is satisfied. Particularly, Armijo's line search satisfies

$$J\left(\chi^k - \tau_k K'(\chi)\right) \geq J(\chi^k) - c_1 \tau_k \nabla J(\chi^k) K_s'(\chi), \quad (10)$$

where $c_1 \in (0, \frac{1}{2})$ and $K_s'(\chi)$ is the search direction such that (10) is satisfied. This concludes that function values satisfy the condition $J(\chi^{k+1}) \leq J(\chi^k)$ impose the monotonicity to the sequence of functions generated by this scheme and this scheme is globally convergent [17].

3) Priori Constraints: Imposing a-priori constraints can improve the quality of solutions to the inverse problems in a great portion [18]. Towards this end, non-negativity is important in applications like imaging [6], [18]. We know that in order to have a physical solution the unknowns we are dealing with should have constraints, the latter being $\epsilon_r(\mathbf{r}) \geq 1$ and $\sigma(\mathbf{r}) \geq 0$. However, in the general case (as embedded obstacle in half-space) those constraints do not impose non-negativity to the real and imaginary parts of the contrast function. We can consider the constraint by "Projection" where at each iteration the following projection $\epsilon_r(\mathbf{r}) = \max(\epsilon_r(\mathbf{r}), 1)$ and $\sigma(\mathbf{r}) = \max(\sigma(\mathbf{r}), 0)$ is applied. Another constraint which can be applied is the way with "Gradient" where two new real-valued unknowns κ and η are introduced as $\varepsilon_r(\mathbf{r}) = 1 + \kappa^2(\mathbf{r})$ and $\sigma(\mathbf{r}) = \eta^2(\mathbf{r})$. The gradient of the cost functional with respect to these two real-valued unknowns being obtained through the classical chain rule from the cost functional with respect to the unknown complex-values $\chi(\mathbf{r})$.

4) Stopping Criteria: There are many ways to choose the stopping criteria. One possible way is to check τ when falling below a small positive constant. It can be interpreted as when maximum absolute value of step size times search direction goes below a small positive constant and this is the way that we are using in our tests in this paper.

IV. Numerical Results

In the following the basis functions ψ_k have been chosen as pixel-based. In our case the true value of the relative permittivity of the object is 2 whereas it is 1 for embedding medium. The scattering object which is dielectric square sided λ (1 m) under the test is contained in a $l = 3 \times \lambda$-sided square investigation area D centered at the origin, and the discretization size is $n \times n = 36 \times 36$ for forward problem and $n \times n = 18 \times 18$ in an inverse problem. The number of transmitters and receivers located around the investigation area are 29 as shown in fig.1. The frequency of the transmitters is 300 MHz. The measured field samples are generated by adding 10 dB white Gaussian noise.

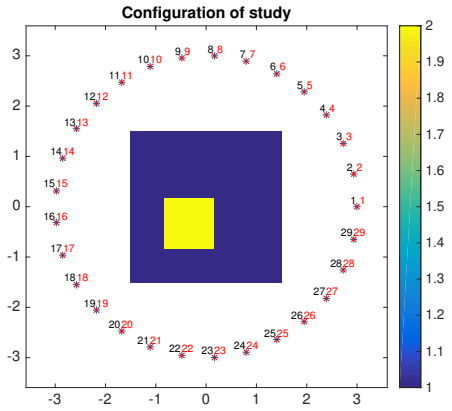

Fig. 1: Measured configuration of actual permittivity profile and source-receiver locations on (x(m), y(m)) axis.

One of the key point of such an inversion is the choice of the regularization parameters α in (7) and β in (8) (δ being kept constant and equal to 1). Different tests have been performed in order to evaluate the sensitivity of the choice of those parameters on the solution. A proper choice of the weighting parameters α and β will allow us to drive the regularization properties of our algorithm in an efficient and predictable way. In order to achieve a reconstruction which is close to the real case we make modifications which affect the parameters. At first we consider the reconstruction as a function of α with a constant β as in fig. 3. Secondly we examine the same reconstruction with a constant α as a function of β as in fig. 2.

In the first case we observe a better reconstruction of the real case by increasing the parameter α such as in figs. 4c and 4d or in figs. 5c and 5d. The higher the value we choose for α the sharper the reconstructions are. However, the choice of α is not arbitrary as can be seen in fig. 3. The error in permittivity gets bigger for larger α. We get a minimum error when α is 2.5×10^{-2}. In the figs. 2 and 3 the relative error norm is calculated as

$$\varepsilon_r^{\text{err}} = \frac{\|\varepsilon_r^{\text{rec}} - \varepsilon_r\|_2}{\|\varepsilon_r\|_2}, \quad (11)$$

whereas $\varepsilon_r^{\text{rec}}$ is the reconstructed permittivity.

In the other case we would expect the inclusion to get smoother when we increase β. However, in fig. 2 it can be observed that there is no crucial differences when β is 1, 1.5 and 2.5 differently than 2. We should choose β carefully and close to one in order not to lose the differentiability for the next iteration. Using β as 1.5 shows that the reconstruction becomes smoother as can be seen in figs. 4e and 5e compared to the figures without any smoothness.

V. Conclusion

Soft iterative thresholding is used to solve the 2-D electromagnetic inverse scattering problem based on l_1 norm penalty term whereas sparsity is enforced by soft shrinkage thresholding function. Retrieval of arbitrary shaped targets from simulated data shows that this approach is effective and

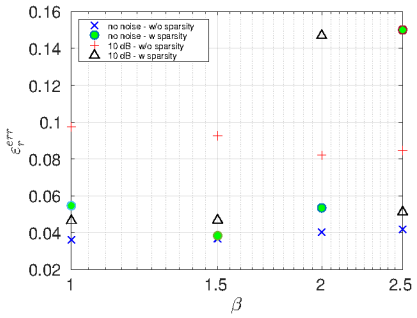

Fig. 2: Error of permittivity w.r.t different values of β when α is equal to 2.5×10^{-2} for the cases with (w) sparsity and without (w/o) sparsity.

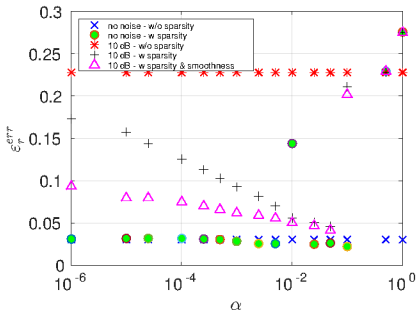

Fig. 3: Error of permittivity w.r.t different values of α when β is equal to 0 for the cases with (w) sparsity, smoothness and without (w/o) sparsity.

gives us reliable insight of dielectric properties of the unknown scatterer and sharper reconstructions by adopting proposed constraints.

Taking advantage of BB method for step size selection enhance the effectiveness and convergence rate of proposed method. Even if choosing the regularization and smoothing parameter is challenging, proper choice can lead us to have reliable reconstructions and compare favorably with those obtained without soft shrinkage enforcement.

Even though the results are promising and advantageous, investigations in experimental settings need to be done to show the feasibility of the algorithm whereas this would be our next step. The development of nonlinear inversion with sparsity regularization for higher permittivity values will be studied.

TABLE I: Average Simulation Time Per Iteration In seconds for noiseless and 10 dB cases

Scenario	Time for noiseless	Time for 10 dB
Without Sparsity	0.5575	0.2260
$\alpha = 2.5 \times 10^{-2}$	0.6168	0.2932
$\beta = 1.5$	0.4305	0.4486
$\alpha = 2.5 \times 10^{-2}$, $\beta = 1.5$	0.4944	0.2442

Moreover, projection constraints will be added to the proposed algorithm as mentioned above. Application into 3-D case with stratified medium will be in our future studies as well.

ACKNOWLEDGMENT

This work is supported by DIGITEO France through the SIRENA project (2014–2017) under the "Call for Chairs."

REFERENCES

[1] L. Poli, G. Oliveri, and A. Massa, "Microwave imaging within the first-order born approximation by means of the contrast-field bayesian compressive sensing," *Antennas and Propagation, IEEE Transactions on*, vol. 60, no. 6, pp. 2865–2879, 2012.

[2] M. Pastorino, *Microwave imaging*. John Wiley & Sons, 2010, vol. 208.

[3] F. Di Benedetto, C. Estatico, J. G. Nagy, and M. Pastorino, "Numerical linear algebra for nonlinear microwave imaging," *Electronic Transactions on Numerical Analysis*, vol. 33, pp. 105–125, 2009.

[4] R. Ramlau and G. Teschke, "A tikhonov-based projection iteration for nonlinear ill-posed problems with sparsity constraints," *Numerische Mathematik*, vol. 104, no. 2, pp. 177–203, 2006.

[5] J. H. Richmond, "Scattering by a dielectric cylinder of abritrary cross-section shape," *IEEE Transactions on Antennas and Propagation*, vol. 13, no. 3, pp. 334–341, 1965.

[6] I. Daubechies, M. Defrise, and C. De Mol, "An iterative thresholding algorithm for linear inverse problems with a sparsity constraint," *arXiv preprint math/0307152*, 2003.

[7] B. Jin and P. Maass, "Sparsity regularization for parameter identification problems," *Inverse Problems*, vol. 28, no. 12, p. 123001, 2012.

[8] M. Grasmair, M. Haltmeier, and O. Scherzer, "Sparse regularization with lq penalty term," *Inverse Problems*, vol. 24, no. 5, p. 055020, 2008.

[9] M. Hanke, A. Neubauer, and O. Scherzer, "A convergence analysis of the landweber iteration for nonlinear ill-posed problems," *Numerische Mathematik*, vol. 72, no. 1, pp. 21–37, 1995.

[10] A. Desmal and H. Bagci, "Sparse electromagnetic imaging using nonlinear landweber iterations," *Progress In Electromagnetics Research*, 2015.

[11] H. Bagci and A. Desmal, "Shrinkage-thresholding enhanced born iterative method for solving 2d inverse electromagnetic scattering problem," *Antennas and Propagation, IEEE Transactions on*, vol. 62, no. 7, pp. 3878–3884, 2014.

[12] M. Gehre, T. Kluth, A. Lipponen, B. Jin, A. Seppänen, J. P. Kaipio, and P. Maass, "Sparsity reconstruction in electrical impedance tomography: an experimental evaluation," *Journal of Computational and Applied Mathematics*, vol. 236, no. 8, pp. 2126–2136, 2012.

[13] B. Jin, T. Khan, and P. Maass, "A reconstruction algorithm for electrical impedance tomography based on sparsity regularization," *International Journal for Numerical Methods in Engineering*, vol. 89, no. 3, pp. 337–353, 2012.

[14] T. Bonesky, K. Bredies, D. A. Lorenz, and P. Maass, "A generalized conditional gradient method for nonlinear operator equations with sparsity constraints," *Inverse Problems*, vol. 23, no. 5, p. 2041, 2007.

[15] P. González-Rodríguez, M. Kindelan, M. Moscoso, and O. Dorn, "History matching problem in reservoir engineering using the propagation–backpropagation method," *Inverse Problems*, vol. 21, no. 2, p. 565, 2005.

[16] J. Barzilai and J. M. Borwein, "Two-point step size gradient methods," *IMA Journal of Numerical Analysis*, vol. 8, no. 1, pp. 141–148, 1988.

[17] L. Grippo, F. Lampariello, and S. Lucidi, "A nonmonotone line search technique for newton's method," *SIAM Journal on Numerical Analysis*, vol. 23, no. 4, pp. 707–716, 1986.

[18] C. R. Vogel, *Computational methods for inverse problems*. SIAM, 2002, vol. 23.

[19] L. Poli, G. Oliveri, F. Viani, and A. Massa, "Mt–bcs-based microwave imaging approach through minimum-norm current expansion," *Antennas and Propagation, IEEE Transactions on*, vol. 61, no. 9, pp. 4722–4732, 2013.

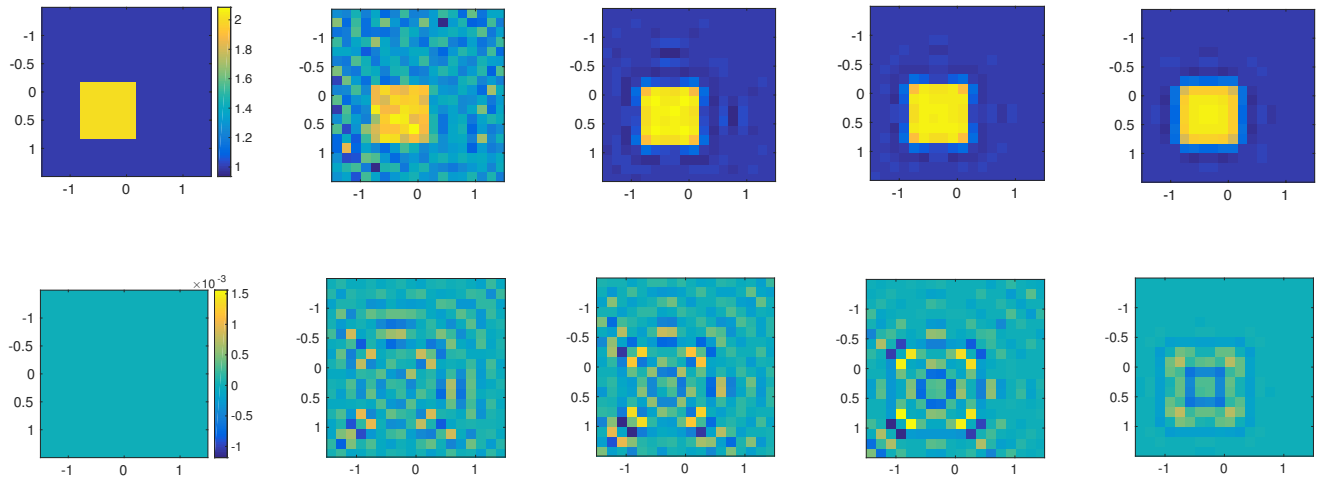

(a) Exact (b) Without sparsity (c) $\alpha = 1 \times 10^{-3}$ (d) $\alpha = 2.5 \times 10^{-2}$ (e) $\alpha = 2.5 \times 10^{-2}$, $\beta = 1.5$

Fig. 4: Retrieval of permittivity ε_r (top) and conductivity σ (bottom) using sparsity and smoothness without noise.

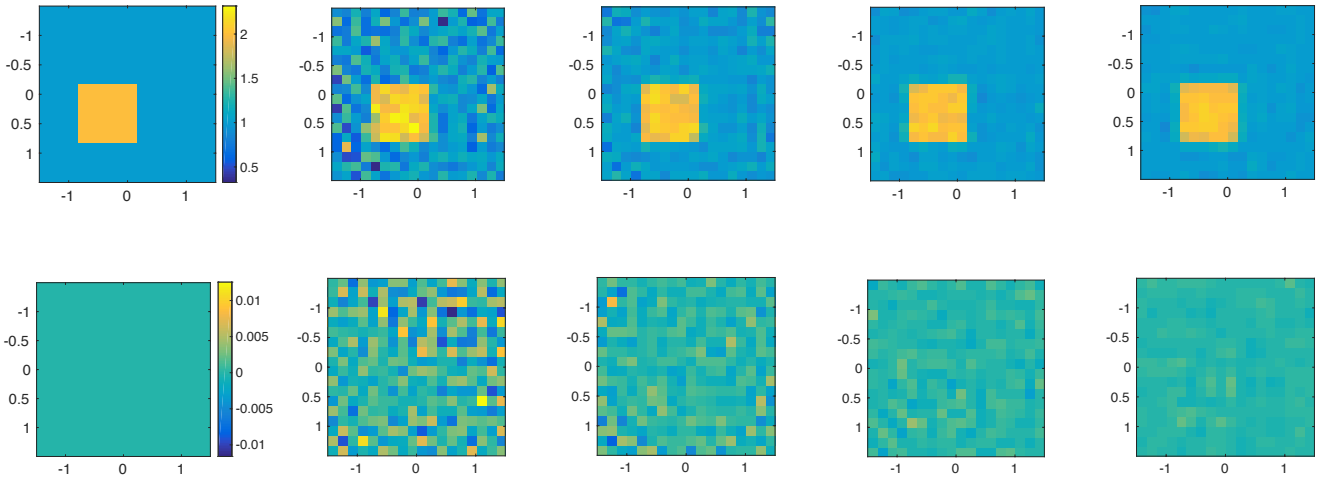

(a) Exact (b) Without sparsity (c) $\alpha = 1 \times 10^{-3}$ (d) $\alpha = 2.5 \times 10^{-2}$ (e) $\alpha = 2.5 \times 10^{-2}$, $\beta = 1.5$

Fig. 5: Retrieval of permittivity ε_r (top) and conductivity σ (bottom) using sparsity and smoothness with $10\,\mathrm{dB}$ noise data.